The Journal of Neuroscience, August 1993, 13(8): 3333–3345

Inward-rectifying Potassium Channels in Retinal Glial (Müller) Cells

Eric A. Newman

Department of Physiology, University of Minnesota, Minneapolis, Minnesota 55455

The voltage- and K^+-dependent properties of Müller cell currents and channels were characterized in freshly dissociated salamander Müller cells. In whole-cell voltage-clamp experiments, cells with endfeet intact and cells missing endfeet both displayed strong inward rectification. The rectification was similar in shape in both groups of cells but currents were 9.2 times larger in cells with endfeet. Ba^{2+} at 100 μM reduced the inward current to 6.8% of control amplitude. Decreasing external K^+ concentration shifted the cell current–voltage (*I–V*) relation in a hyperpolarizing direction and reduced current magnitude. In multichannel, cell-attached patch-clamp experiments, patches from both endfoot and soma membrane displayed strong inward rectification. Currents were 38 times larger in endfoot patches. In single-channel, cell-attached patch-clamp experiments, inward-rectifying K^+ channels were, in almost all cases, the only channels present in patches of endfoot, proximal process, and soma membrane. Channel conductance was 27.8 pS in 98 mM external K^+. Reducing external K^+ shifted the channel reversal potential in a hyperpolarizing direction and reduced channel conductance. Channel open probability varied as a function of voltage, being reduced at more negative potentials. Together, these observations demonstrate that the principal ion channel in all Müller cell regions is an inward-rectifying K^+ channel. Channel density is far higher on the cell endfoot than in other cell regions.

Whole-cell *I–V* plots of cells bathed in 12, 7, 4, and 2.5 mM K^+ were fit by an equation including Boltzmann relation terms representing channel rectification and channel open probability. This equation was incorporated into a model of K^+ dynamics in the retina to evaluate the significance of inward-rectifying channels to the spatial buffering/K^+ siphoning mechanism of K^+ regulation. Compared with ohmic channels, inward-rectifying channels increased the rate of K^+ clearance from the retina by 23% for a 1 mM K^+ increase and by 137% for a 9.5 mM K^+ increase, demonstrating that Müller cell inward-rectifying channels enhance K^+ regulation in the retina.

[Key words: glial cell, Müller cell, inward-rectifying potassium channel, voltage clamp, salamander, potassium homeostasis]

An essential function of glial cells is to regulate extracellular K^+ levels, $[K^+]_o$, in the CNS (Newman, 1985a; Cserr, 1986). One of the mechanisms by which this is accomplished is "potassium spatial buffering" (Orkand et al., 1966; Gardner-Medwin, 1983; Newman et al., 1984; Karwoski et al., 1989). In this process, K^+ is transferred by a current flow through glial cells, from regions where $[K^+]_o$ is higher to regions where $[K^+]_o$ is lower. Potassium spatial buffering currents in glial cells pass through K^+ channels, which dominate the membrane conductance of these cells (Kuffler et al., 1966; Newman, 1985b).

In some types of glial cells, K^+ channels are not distributed uniformly over the cell surface but rather are localized to conductance "hot spots." This is well documented for Müller cells, the principal glial cells of the vertebrate retina. In amphibian Müller cells, K^+ conductance is localized to the cell endfoot, a structure that lies adjacent to the vitreous humor (Newman, 1984, 1987; Brew et al., 1986). In mammalian Müller cells, additional high-conductance regions are present elsewhere over the cell surface (Newman, 1987). Similarly, in astrocytes from the amphibian optic nerve, cell endfeet have approximately a tenfold higher specific K^+ conductance than do other regions of the cell (Newman, 1986).

We have proposed that the high K^+ conductance of glial cell endfeet results in a specialized and more efficient form of K^+ spatial buffering termed "K^+ siphoning" (Newman et al., 1984). In this process, spatial buffering currents in glial cells are selectively directed out through the cell endfeet. In the amphibian retina, Müller cells are believed to regulate light-evoked changes in $[K^+]_o$ by this process (Karwoski et al., 1989).

The type or types of K^+ channels that mediate K^+ siphoning currents may have an important influence on this homeostatic process. Is the high K^+ conductance of the Müller cell endfoot mediated by the same K^+ channel responsible for the conductance of other cell regions? Do the voltage-dependent properties of the channels influence the magnitude of K^+ siphoning currents? Answers to these questions are needed to understand the role that glial cells play in the regulation of $[K^+]_o$.

A previous study utilizing single-channel recordings has demonstrated that the principal K^+ channel in both endfoot and non-endfoot regions of amphibian Müller cells is an inward-rectifying K^+ channel (Brew et al., 1986). This channel has a high open probability, and consequently, a large macroscopic conductance, at the resting membrane potential of the cell (Brew et al., 1986). In contrast, fast-inactivating (type A) K^+ channels and Ca^{2+}-activated K^+ channels, which are also present in Müller cells (Newman, 1985c), have a low open probability at the cell resting potential.

Although an inward-rectifying K^+ channel is thought to be the primary channel open at rest in Müller cells, channel currents have not been characterized in these cells using the whole-cell

Received Oct. 5, 1992; revised Jan. 4, 1993; accepted Feb. 18, 1993.

I thank Paul W. Ceelen for his excellent technical assistance and Janice I. Gepner, Kathleen R. Zahs, and Davida Z. Streett for their helpful comments on the manuscript. This work was supported by National Institutes of Health Grant EY 04077.

Correspondence should be addressed to Dr. Eric A. Newman, 6-255 Millard Hall, Department of Physiology, University of Minnesota, 435 Delaware Street S.E., Minneapolis, MN 55455.

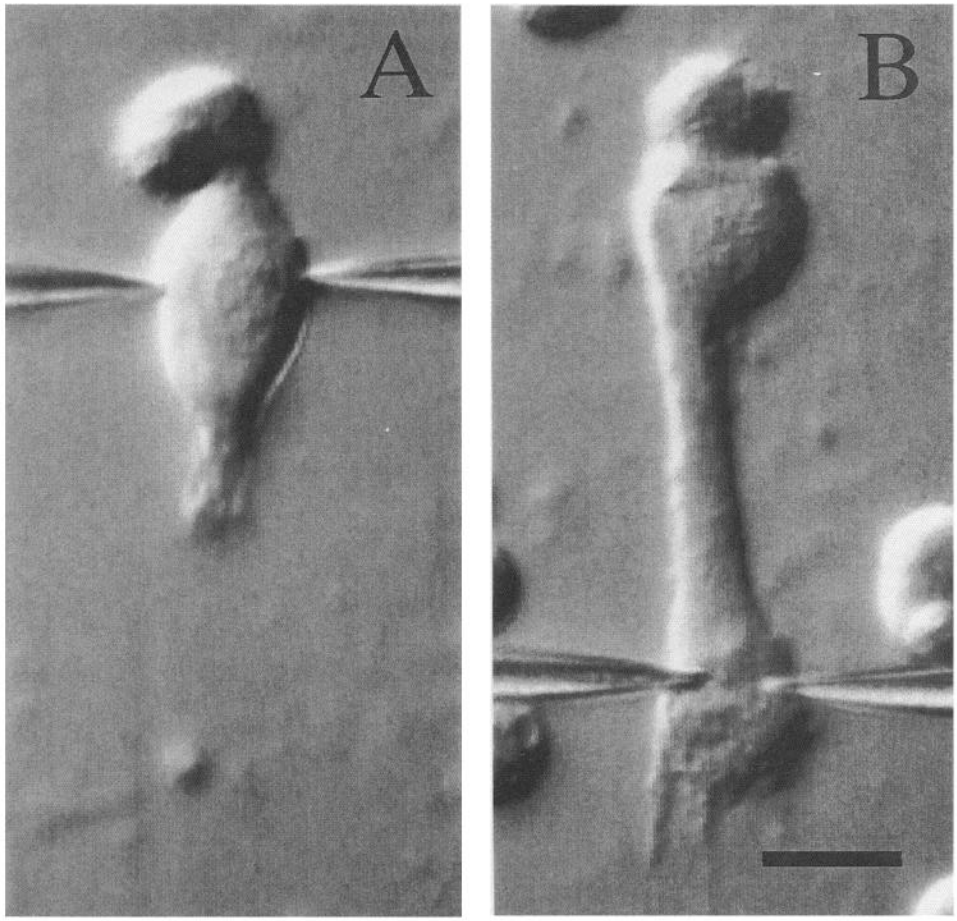

Figure 1. Micrographs of dissociated salamander Müller cells. *A*, Cell without an endfoot. The endfoot and a portion of the proximal process were sheared off during the isolation procedure. Both voltage-sensing and current-passing voltage-clamp pipettes are patched onto the soma. *B*, Cell with endfoot intact. Both recording pipettes are patched onto the endfoot. Nomarski differential interference optics. Scale bar, 20 μm.

voltage-clamp technique. In addition, the voltage- and K^+-dependent properties of channel currents have not been quantitatively described. Such a description is needed to evaluate how this channel will influence the process of K^+ siphoning.

The goals of this work are threefold: first, to confirm that an inward-rectifying K^+ channel is the primary channel that conducts current in both endfoot and non-endfoot regions of amphibian Müller cells; second, to obtain a quantitative description of inward-rectifying K^+ channel properties; and third, to assess how these properties influence K^+ regulation in the retina. I have used whole-cell voltage-clamp, multichannel patch-clamp, and single-channel patch-clamp recordings to confirm the presence and to characterize the properties of K^+ channels in endfoot and non-endfoot regions of salamander Müller cells. These channel properties were then incorporated into a model of K^+ dynamics in the retina to evaluate the effect of the channel on glial cell regulation of $[K^+]_o$.

A preliminary report of some of these findings has appeared previously (Newman, 1989b).

Materials and Methods

Animals. Tiger salamanders (*Ambystoma tigrinum*, aquatic stage) were used. Animals were killed by decapitation and pithing.

Cell dissociation. Recordings were made from freshly dissociated cells. The cell dissociation procedure has been described previously (Newman, 1985b) and yields cells with membrane properties similar to those of *in situ* cells. Briefly, isolated retinas from hemisected eyes were incubated in Ca^{2+}-, Mg^{2+}-free Ringer's solution containing papain (35 units of activity/3 ml) and cysteine (2 mM). The tissue was incubated for 20–30 min at 22°C while being triturated gently at 5 min intervals. The tissue was then rinsed twice in normal Ringer's containing 1% BSA and twice more in Ringer's containing 1% BSA and 0.1% DNase. The tissue was maintained in the final rinse solution at 0°C for a period of 3–6 hr and was then triturated using a series of Pasteur pipettes with progressively smaller tip openings.

Dissociated cells were placed in a perfusion chamber and settled onto a glass slide coated with concanavalin-A. The perfusion chamber had a volume of ~0.25 ml and was perfused at a rate of ~1.5 ml/min. Cells were maintained at 15–17°C in the perfusion chamber. Recordings were made from cells within 2 hr of dissociation.

Most isolated cells possessed endfeet and some lateral processes (Fig. 1*B*). In some cells, however, the endfoot and a portion of the proximal process were missing, having been torn off during the isolation procedure (Fig. 1*A*). As demonstrated previously (Newman, 1985b), these cells without endfeet are viable and have normal resting potentials.

Whole-cell voltage clamp. Müller cells were voltage clamped employing the two-electrode clamp technique with patch pipettes used in the whole-cell recording configuration (Hamill et al., 1981). Patch pipettes had a tip inner diameter of ~1 μm and were coated with Sylgard to reduce cross-capacitance coupling.

Both command pulse and command ramp protocols were used to measure whole-cell currents. Two ramp speeds were used, a fast ramp of 2750 mV/sec and a slow ramp of 68.75 mV/sec. Ramps began at a negative membrane potential and were swept in a positive direction. The first 20 mV of ramp records were discarded to avoid the transient artifact generated by the hyperpolarizing step from the holding potential.

Cell-attached patch clamp. Both multi-channel and single-channel patch-clamp recordings were obtained using the cell-attached recording configuration (Hamill et al., 1981). Patch pipettes were coated with Sylgard and had an inner diameter of ~0.8 μm for multichannel recordings and ~0.4 μm for single-channel recordings.

The membrane voltages specified for cell-attached patch recordings are corrected for the membrane potential of the cell, which was deter-

mined to be −74.9 ± 1.6 mV (mean ± SD; n = 55) in a series of recordings in an external solution containing 2.5 mM K^+ (perfusate B). A specified membrane potential of −20 mV corresponds to an actual transmembrane potential of −20 mV (inside negative) and to a potential of −55 mV applied to the pipette.

Amplifiers and data acquisition. An Axoclamp-2A amplifier (Axon Instruments) was used for the two-electrode, whole-cell voltage-clamp recordings. An Axopatch-1C amplifier with a CV-4 headstage (Axon Instruments) was used for cell-attached patch recordings. Records were acquired and displayed on a digital oscilloscope and stored in an IBM-compatible microcomputer. Whole-cell and multichannel voltage-clamp recordings were filtered at 500 Hz (80 dB/decade Bessel filter). For single-channel recordings, CLAMPEX and FETCHEX programs (pClamp software, Axon Instruments) were used to acquire and store data. Single-channel records were digitally sampled at 2 kHz and filtered at 1 kHz.

Solutions. The composition of the solutions used (in mM) is as follows.

Perfusate A, bath perfusate for whole-cell voltage-clamp experiments with $[K^+]_o$ = 98 mM, contained KCl, 98.0; *N*-methyl-D-glucamine-Cl, 3.3; $CaCl_2$, 1.8; $MgCl_2$, 0.8; $CdCl_2$, 2.0; dextrose, 10; HEPES, 10. pH was adjusted to 7.5 with *N*-methyl-D-glucamine. The $CaCl_2$ was omitted in some experiments. For experiments with 2.5, 10, and 30 mM $[K^+]_o$, *N*-methyl-D-glucamine-Cl was substituted for KCl. The Cd^{2+} served to block Ca^{2+} influx and activation of Ca^{2+}-gated K^+ channels. Cd^{2+} reduced outward K^+ currents in whole-cell voltage-clamp experiments but had no effect on inward currents.

Perfusate B was used as bath perfusate for whole-cell voltage-clamp experiments with $[K^+]_o$ = 2.5–12 mM. For $[K^+]_o$ = 2.5 mM, it contained KCl, 2.5; NaCl, 98.5; $CaCl_2$, 1.8; $MgCl_2$, 0.8; dextrose, 10; HEPES, 10. pH was adjusted to 7.5 with NaOH. For $[K^+]_o$ = 4, 7, and 12 mM, KCl was substituted for NaCl.

Pipette (internal) solution for whole-cell voltage-clamp experiments contained KCl, 98.0; $MgCl_2$, 0.8; HEPES, 10. pH was adjusted to 7.1 with *N*-methyl-D-glucamine.

Pipette (external) solution for cell-attached patch-clamp experiments with $[K^+]$ = 98 mM contained KCl, 98.0; NaCl, 3.0; $CaCl_2$, 1.8; $MgCl_2$, 0.8; dextrose, 10; HEPES, 10. pH was adjusted to 7.5 with NaOH. For $[K^+]$ = 30 and 10 mM, NaCl was substituted for KCl.

Bath perfusate B (2.5 mM K^+) was used as the bath solution in cell-attached patch-clamp experiments.

Analysis. Except when otherwise noted, results are given as the mean ± standard deviation (sample number in parentheses).

Curve fitting was achieved using the nonlinear regression Marquardt–Levenberg algorithm (Sigmaplot software, Jandel Scientific). Current–voltage relations and the channel open probability versus voltage relation were analyzed by fitting records to the two-state Boltzmann equation. Details are given in Results.

Single-channel records were analyzed by converting them to current amplitude histograms (using FETCHAN, pClamp software, Axon Instruments), which were fit to the sum of several Gaussians. The amplitude probability of the histograms, P_I, has the form

$$P_I = \sum_{j=0}^{n} P_j \cdot G_j, \tag{1}$$

$$G_j = \exp\left(\frac{-(\mathrm{AMP}_{\mathrm{ZERO}} + j\cdot\Delta\mathrm{AMP} - I)^2}{\sigma^2}\right), \tag{2}$$

$$P_j = \frac{n!}{(n-j)!\cdot j!}(P_o)^j\cdot(1 - P_o)^{(n-j)}, \tag{3}$$

where the jth term in Equation 1 represents the instance when j channels are open and n is the total number of channels in the patch. G_j is the Gaussian relation for the jth term and P_j is the probability value for the jth term. $\mathrm{AMP}_{\mathrm{ZERO}}$ is the current value when all channels are closed, ΔAMP is the channel unitary current, I is the channel current, σ is the standard deviation of the Gaussian, and P_o is the channel open probability. Equations 1–3 were fit to the current amplitude histograms of individual patch records with parameters ΔAMP, P_o, $\mathrm{AMP}_{\mathrm{ZERO}}$, and σ varied to provide the best fit.

Model of K^+ dynamics in the retina. Clearance of K^+ from the retina was evaluated using a model of K^+ dynamics described previously (Odette and Newman, 1988). Model parameters were identical to those specified in an earlier study (Karwoski et al., 1989) except for the following: (1) Müller cell conductance (exclusively K^+) was either ohmic or inward rectifying. In the latter case, cell conductance was specified by Equation 10, below. (2) Eighty-nine percent of the total conductance of Müller cells was assumed to lie in the endfoot and ganglion cell layers. (3) There was no passive or active uptake of K^+. (4) At time = 0, $[K^+]_o$ was raised instantaneously and uniformly within the inner plexiform layer.

Results

Whole-cell current–voltage relation

The endfoot of amphibian Müller cells has a substantially higher K^+ conductance than do other cell regions (Newman, 1985b). Is this high conductance due to the presence of a high density of the same K^+ channel found in other cell regions, or is it due to the presence of a K^+ channel unique to the endfoot? This question was addressed by determining the *I–V* characteristics of the membrane of endfoot and non-endfoot regions of salamander Müller cells.

In order to determine the *I–V* relation of the non-endfoot membrane of Müller cells, whole-cell voltage-clamp experiments were performed on dissociated cells lacking their endfeet (Fig. 1*A*). The endfeet and proximal processes of these cells had been sheared off during the dissociation procedure. The *I–V* relation of the endfoot region of Müller cells, in contrast, was determined by performing whole-cell voltage-clamp experiments on dissociated cells with their endfeet intact (Fig. 1*B*). Since a large fraction of the total cell conductance is contained in the endfoot, the *I–V* relations of these cells largely reflect the properties of the endfoot membrane.

For cells both with and without endfeet, a two-electrode voltage clamp was employed. Both voltage-sensing and current-passing pipettes were placed on the cell soma when recording from cells without endfeet (Fig. 1*A*). The two pipettes were placed on the cell endfoot when recording from cells with endfeet intact (Fig. 1*B*). As will be demonstrated below, the placement of both pipettes on the endfoot was essential for obtaining a good space clamp and achieving accurate *I–V* plots. Cells were bathed in a solution containing 98 mM K^+ and were internally dialyzed with a pipette solution also containing 98 mM K^+. Under these conditions, the resting membrane potential was near 0 mV.

Voltage-clamp records, both from Müller cells lacking their endfeet (Fig. 2*A*) and from cells with their endfeet intact (Fig. 2*B*), showed strong inward rectification. In both cases, hyperpolarizing voltage pulses yielded large inward currents while depolarizing pulses produced far smaller outward currents. For large hyperpolarizations, the inward current peaked rapidly and then declined to a smaller, sustained value.

In Figure 2, the amplitudes of the voltage-clamp responses shown in *A* and *B* are plotted as a function of command voltage in *C* and *D*. Both peak current (solid circles) and sustained current (open circles) are shown. The degree of rectification was similar for both cells. However, the magnitudes of the currents were dramatically different. Evoked currents were substantially larger for the cell with its endfoot intact compared to the cell without its endfoot.

A quantitative comparison of current amplitudes was conducted by measuring the peak currents evoked for −100 mV command pulses. Current amplitude was −148.9 ± 47.0 nA (n = 27) for cells with endfeet, and −16.1 ± 8.5 nA (n = 22) for cells without endfeet. Based on this current amplitude measure, 89.2% of the total cell conductance is contained within the endfoot and adjacent portions of the proximal cell process, those portions of the cell missing in cells lacking endfeet. This is a

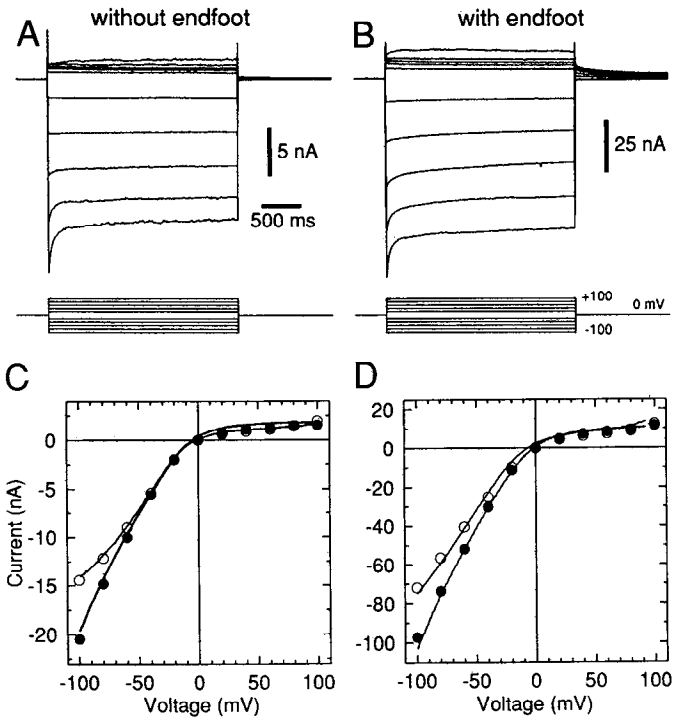

Figure 2. Whole-cell voltage clamp of dissociated Müller cells. *A* and *B*, Voltage-clamp records of a cell without an endfoot (*A*), and a cell with endfoot intact (*B*). The clamp protocol, illustrated at the bottom of the traces, consists of 2.4 sec pulses with amplitudes varying from −100 mV to +100 mV in 20 mV increments. Holding potential for both cells, 0 mV. *C* and *D*, *I–V* relations plotted from the voltage-clamp records in *A* and *B*. *Solid circles*, peak current amplitude; *open circles*, sustained current amplitude (measured at the end of the 2.4 sec command pulse). The *continuous lines* are *I–V* relations of the same two cells, obtained using command voltage ramps. The *lines superimposed over the solid circles* were obtained using fast ramps. The *lines superimposed over the open circles* were obtained using slow ramps. The *I–V* relations obtained using command pulse and command ramp protocols are nearly identical. The *I–V* plots of the two cells show strong inward rectification. The plots have a similar form, but current amplitudes are approximately fivefold larger for the cell with its endfoot intact.

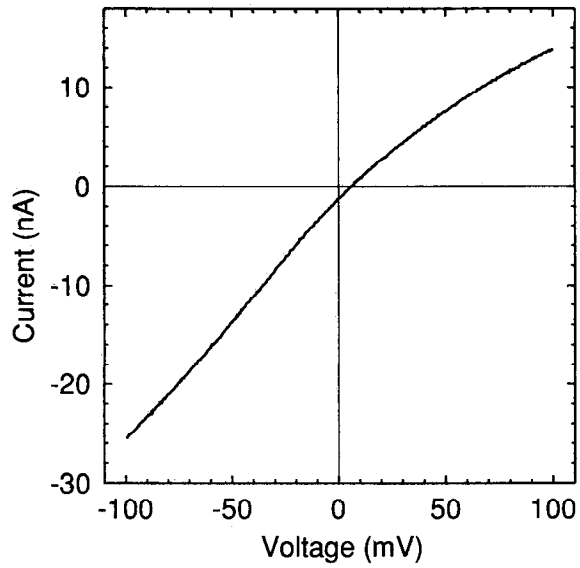

Figure 3. Distortion of the *I–V* relation of a Müller cell with endfoot when recording pipettes are patched onto the cell soma. Placing the two voltage-clamp pipettes on the soma results in poor space clamp and a grossly distorted *I–V* relation, which appears to be almost linear. An *I–V* plot with strong inward rectification would have been obtained if the two pipettes had been patched onto the endfoot. Slow ramp protocol. Holding potential, +7 mV.

somewhat lower percentage than the 95% value obtained in an earlier study (Newman, 1985b).

The *I–V* relations obtained from cells with and without endfeet were fit by Equations 4–7, which incorporate the two-state Boltzmann relation (Eq. 7), in order to compare their shapes quantitatively (Hagiwara and Takahashi, 1974; Hagiwara, 1983; Oliva et al., 1990). The equations have the form

$$I = \Delta V \cdot g, \tag{4}$$

$$\Delta V = V - E_K, \tag{5}$$

$$E_K = N_{SLOPE} \cdot \ln\left(\frac{[K^+]_o}{[K^+]_i}\right), \tag{6}$$

$$g = c \cdot \left[1 + \exp\left(\frac{\Delta V - V_h^R}{S^R}\right)\right]^{-1}, \tag{7}$$

where I is the membrane current, ΔV is the driving force for K^+ flux, E_K is the Nernst potential for K^+, N_{SLOPE} is the Nernst constant, and g is the membrane conductance. c is a scaling constant, V_h^R is the voltage at which the conductance is half-maximal, and S^R is a measure of the rate at which the conductance changes with voltage. The magnitude of cell rectification (the ratio of inward to outward current) is described well by the parameter S^R, while V_h^R specifies the voltage at which the rectification occurs (the location of the shoulder of the *I–V* plot). The parameters S^R, V_h^R, and c were varied to obtain the best fits for *I–V* plots of peak current.

The calculated values of the parameter S^R were nearly identical for cells with and without endfeet. Mean values of S^R were 33.8 ± 4.2 mV (12) and 32.2 ± 6.1 mV (9), respectively, indicating that the *I–V* relations of the two groups of cells rectified to the same degree. Mean values of the parameter V_h^R were −13.9 ± 8.5 mV (12) and −21.4 ± 6.1 mV (9) for cells with and without endfeet.

The *I–V* characteristics of Müller cells were determined by utilizing command ramps of voltage as well as command pulses. Two ramp speeds were employed, a fast ramp of 2750 mV/sec and a slow ramp of 68.75 mV/sec.

Currents evoked by fast and slow command ramps are illustrated in Figure 2, *C* and *D* (continuous lines), along with the *I–V* relations from the same cells determined using command pulses (symbols). For both cells, rapid ramp currents were nearly identical to the *I–V* relations for peak current derived from command pulses (Fig. 2, solid circles). In a like manner, the slow ramp currents were very similar to the sustained current *I–V* relation derived from pulses (Fig. 2, open circles). This correspondence is reasonable. A rapid ramp sweeps through the entire voltage range before the cell current has time to decline. Thus, the current evoked by the fast ramp corresponds to the peak current. A slow ramp, on the other hand, essentially measures the steady-state, or sustained current. The similarity between the *I–V* relations determined by command ramps and command pulses demonstrates that cell membrane properties can be assessed accurately using the ramp protocol.

In the voltage-clamp experiments described above, both voltage-sensing and current-passing pipettes were patched onto the

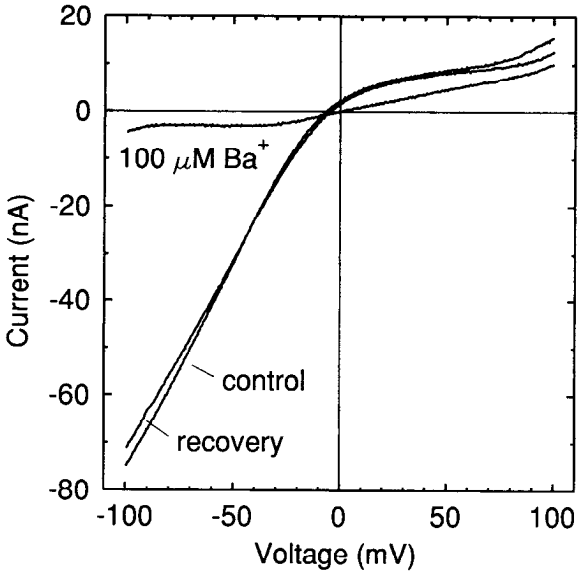

Figure 4. Barium block of inward-rectifying current. Addition of 100 μM Ba^{2+} almost completely abolishes the inward current present in the control trace. The inward current recovers almost completely after 105 sec of washout. Cell with endfoot. Slow ramp protocol. Holding potential, 0 mV.

endfoot when recording from cells with endfeet (Fig. 1*B*). This was done to ensure that the cells were adequately space clamped, an important consideration, particularly when recording from cells that generate large currents. If, in contrast, recordings are made with the two pipettes placed on the cell soma, adequate space clamp is not achieved and the resulting *I–V* relation is grossly distorted. This is illustrated in Figure 3, which shows the *I–V* relation obtained from a cell with the two recording pipettes placed on the soma. The current, instead of displaying marked inward rectification, appears to be almost ohmic. This distortion of the *I–V* plot, arising from improper placement of the recording pipettes, is the reason why I erroneously identified the conductance of the Müller cell endfoot as nonrectifying in previous preliminary publications (Newman, 1985c; Maranto and Newman, 1988).

Barium block of current

The *I–V* relations illustrated in Figure 2 suggest that Müller cell currents are generated principally by inward-rectifying K^+ channels. These channels are known to be blocked by low concentrations of Ba^{2+} (Rudy, 1988; Hille, 1992). Ba^{2+} has also been shown to block the resting conductance of amphibian Müller cells in current-clamp experiments (Newman, 1989a). Müller cell sensitivity to Ba^{2+} was tested in an experiment illustrated in Figure 4, which shows that 100 μM Ba^{2+} almost completely abolishes the inward current present in the control trace. The small remaining current shows modest outward rectification. In a series of such experiments, 100 μM Ba^{2+} reduced the current evoked at −100 mV to 6.8 ± 1.2% (8) of its control magnitude. Current amplitude following recovery was 94.3 ± 9.5% (8) of control.

Potassium dependence of current

Inward-rectifying K^+ channels are sensitive to $[K^+]_o$ as well as to voltage (Hagiwara et al., 1976; Hille, 1992). The sensitivity of Müller cell currents to $[K^+]_o$ was tested by determining cell *I–V* relations sequentially in bath solutions containing 98, 30, 10, and 2.5 mM K^+ (Fig. 5*A*). A fast ramp protocol was employed. With each bath solution, the voltage-clamp holding potential was adjusted to the resting (zero current) potential.

Two important changes occurred in the cell *I–V* relation as $[K^+]_o$ was lowered. First, the relations shifted to the left, with both the reversal potential and the shoulder potential having progressively more negative values as $[K^+]_o$ was lowered. Second, the conductance of the cell (the slope of the curve) was reduced for lower $[K^+]_o$.

Both of these changes are typical of currents generated by inward-rectifying K^+ channels (Hagiwara, 1983). The shift in the reversal potential of the current had a slope of 52.5 mV per tenfold change in $[K^+]_o$ ($n = 11$). This slope, close to the Nernstian value of 57 mV, indicates that the channels conducting the current are almost exclusively permeable to K^+.

The reduction in conductance with decreased $[K^+]_o$ is also typical of inward-rectifying K^+ channels and is predicted by the Goldman-Hodgkin-Katz current equation (Hille, 1992). It results from a paucity of charge carriers at reduced $[K^+]_o$; for low

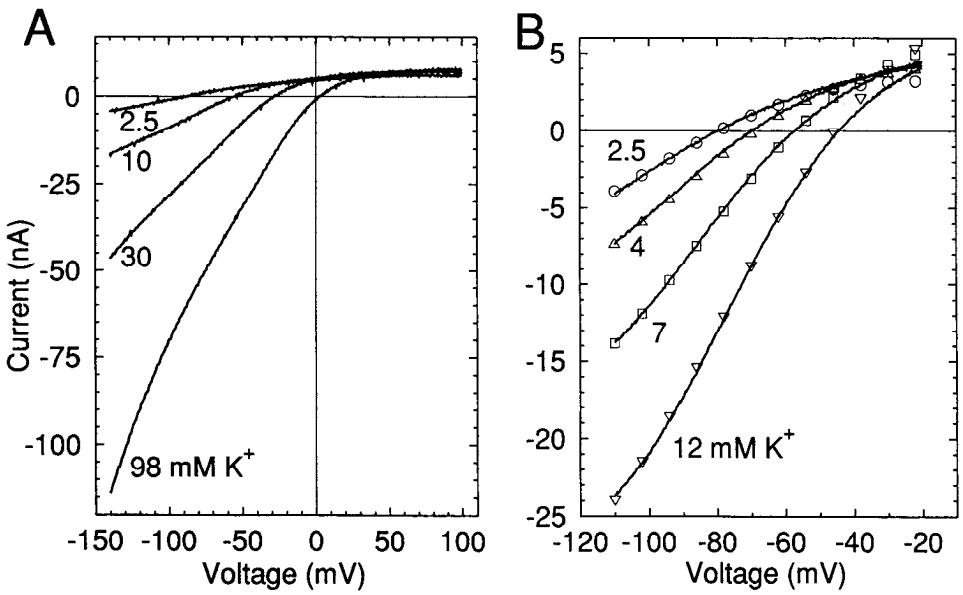

Figure 5. Potassium dependence of whole-cell *I–V* relations. *A*, $[K^+]_o$ is lowered sequentially from 98 mM to 2.5 mM. Cell with endfoot. Fast ramp protocol. Holding potentials, +4, −26, −53, and −83 mV, in 98, 30, 10, and 2.5 mM K^+. *B*, $[K^+]_o$ is lowered sequentially from 12 mM to 2.5 mM. *I–V* relations are shown by *continuous lines*. Cell with endfoot. Slow ramp protocol. Holding potentials, −42, −56, −69, and −79 mV in 12, 7, 4, and 2.5 mM K^+. The *I–V* relations in *B* are fit by Equations 4–6 and 9 with Boltzmann parameters V_h^R *and* S^R equaling −24.0 mV and 45.4 mV, respectively. The theoretical relations (shown by the four sets of symbols) provide an excellent fit, deviating from the experimental records only at the most depolarized voltages. In both *A* and *B*, the conductance of the membrane is reduced and the *I–V* plots shifted to the left as $[K^+]_o$ is reduced.

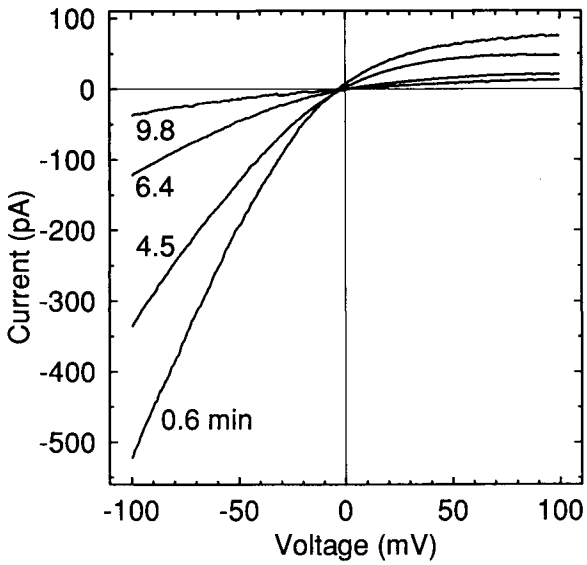

Figure 6. Current–voltage relations of a multichannel patch of endfoot membrane. Trace labels indicate the time (in min) after a tight seal was made. The magnitude of the inward-rectifying current decreases with time. Cell-attached patch. Fast ramp protocol. Holding potential, 0 mV. (−75 mV applied to the patch pipette; see Materials and Methods).

$[K^+]_o$, there are fewer K^+ ions to carry current into the cell. In other systems, the magnitude of inward-rectifying current is approximately proportional to the square root of $[K^+]_o$ (Hagiwara and Takahashi, 1974; Sakmann and Trube, 1984a). The currents recorded from Müller cells held closely to this square root relation (graph not shown).

A second series of recordings were made to determine the K^+ dependence of the *I–V* relations under more physiological conditions (Fig. 5*B*). Recordings were made from Müller cells bathed in solutions containing 12, 7, 4, and 2.5 mM K^+. Recordings also differed from those shown in Figure 5*A* in that slow, rather than fast, command ramps were employed. Thus, the responses correspond to the sustained component rather than the peak component of channel current. Sustained current is more meaningful physiologically than is peak current, because activity-dependent variations in glial cell potentials and in external $[K^+]$ occur relatively slowly in the CNS (Orkand et al., 1966; Kelly and Van Essen, 1974; Karwoski and Proenza, 1980). As in the experiment illustrated in Figure 5*A*, the reversal potential of the *I–V* curve shifted in an hyperpolarizing direction and the conductance of the cell was reduced with decreased $[K^+]_o$. The shift in reversal potential was nearly Nernstian, having a slope of 50.0 mV per decade change in $[K^+]_o$ (n = 13).

Current–voltage relation of membrane patches

The whole-cell voltage-clamp recordings described above indicate that the membrane of both endfoot and non-endfoot regions of Müller cells have similar inward-rectifying conductance properties. This conclusion was tested directly by measuring the *I–V* properties of discrete patches of membrane using the cell-attached patch-clamp technique. These experiments were conducted using multichannel, rather than single-channel, patches in order to obtain the averaged *I–V* relation of many channels at once. Patch pipettes were filled with a solution containing 98 mM K^+.

The voltage-clamp records obtained from a cell-attached membrane patch on the endfoot of a Müller cell are illustrated in Figure 6. Record "0.6 min" was obtained soon after a gigaohm seal was obtained. The current shows pronounced inward rectification. The magnitude of the current is extremely large for a patch recording. As will be demonstrated below, the response represents the summed current of approximately 200 inward-rectifying K^+ channels.

The traces in Figure 6 represent a time series, with the labels indicating the time at which each trace was acquired (in min), relative to the time the gigaohm seal was made. As time proceeds, the magnitude of the current recorded from the patch is reduced. This decline was typical of multichannel patch recordings and was often more rapid than that illustrated in Figure 6. Presumably, the number of active channels in the patch is reduced with time. Although the cause of the loss of active inward-rectifying channels is not known, the phenomenon has been observed in other preparations, including chick lens epithelia (J. L. Rae, personal communication).

The phenomenon of channel loss can be used to advantage. If the *I–V* trace obtained late in a patch recording is subtracted from a trace obtained early on (trace 0.6 minus trace 9.8 in this example), the *I–V* relation of those channels lost in the intervening time is obtained. The advantage of this procedure is that the leakage current of the seal, which is present in both traces, is subtracted out, leaving a more accurate representation of channel *I–V* characteristics. The "difference" *I–V* relations obtained from successive time points (trace 0.6 minus trace 4.5,

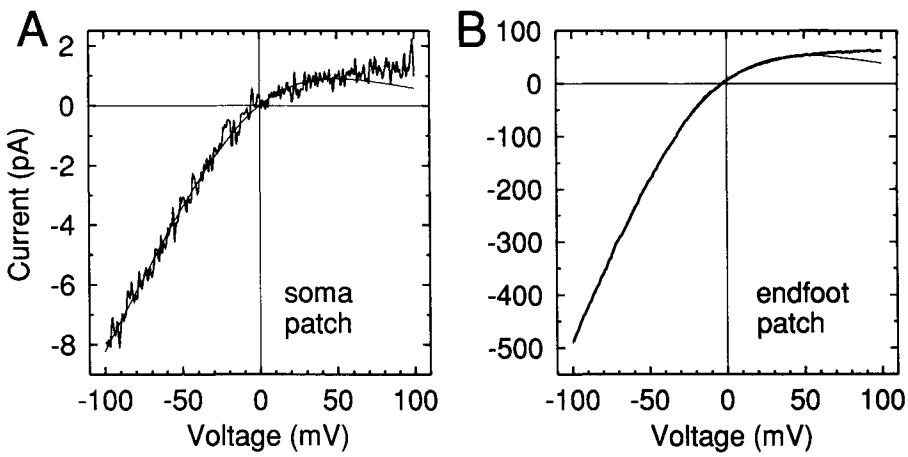

Figure 7. Current–voltage relations of multichannel membrane patches. *A*, Soma membrane patch. *B*, Endfoot membrane patch. The two *I–V* plots show similar inward rectification but vastly different current magnitudes. The current recorded from the endfoot patch is 62 times greater than the current from the soma patch. The *thin lines* show a Boltzmann relation (Eqs. 4–7) fit to the data. (In *B*, the Boltzmann line is superimposed over the voltage-clamp record for most of its length.) Values of Boltzmann parameters V_h^R *and* S^R are −3.3 mV and 38.9 mV in *A* and −19.3 mV and 45.4 mV in *B*. Leakage currents were subtracted from traces (see text). Cell-attached patches. Fast ramp protocol. Holding potentials, 0 mV.

trace 4.5 minus trace 6.4, etc.) had nearly identical shapes, indicating that the membrane patch contained but a single type of channel (graph not shown).

The subtraction procedure was used in analyzing a series of patch recordings. Two examples are illustrated, one from the soma of a cell (Fig. 7*A*) and the other from the endfoot of a second cell (Fig. 7*B*). Both voltage-clamp recordings show marked inward rectification and resemble the *I–V* relations obtained in whole-cell recordings. The two cell-attached patch recordings illustrated in Figure 7 resemble each other closely in form, but differ dramatically in magnitude. The current recorded from the endfoot membrane patch is 60 times larger than is the current from the soma patch.

This difference in current magnitude was found in all recordings and indicates that channel density is higher at the endfoot. In a series of patch recordings from soma membrane, mean current at −100 mV was −7.4 ± 8.0 pA (10). In contrast, patch recordings from endfoot membrane had a mean current of −282 ± 219 pA (17). The ratio of these two values, 38:1, demonstrates that the density of inward-rectifying K^+ channels is far greater on the endfoot than it is on the soma. This ratio actually underestimates the relative density of channels on endfoot and soma membrane for the following reasons. Although the mean current of endfoot patches was −282 pA, the current exceeded −400 pA in 5 out of the 17 patches examined and reached −890 pA in one patch. In addition, many patches on the soma had no channels at all and these were *not* included in the soma average of −7.4 pA. (Comparisons of current amplitude from individual patches are further complicated by the fact that membrane area undoubtedly varied from patch to patch.)

The shapes of the *I–V* relations obtained from soma and endfoot patches were compared quantitatively by fitting the voltage-clamp records with the Boltzmann relation (Eqs. 4–7). Calculated values of the Boltzmann parameter S^R were similar for soma and endfoot patches. Mean values were 48.1 ± 19.7 mV (10) and 43.3 ± 6.2 mV (18), respectively. Mean values for V_h^R were −14.7 ± 37.2 mV (10) and −16.6 ± 18.0 mV (18) for soma and endfoot patches.

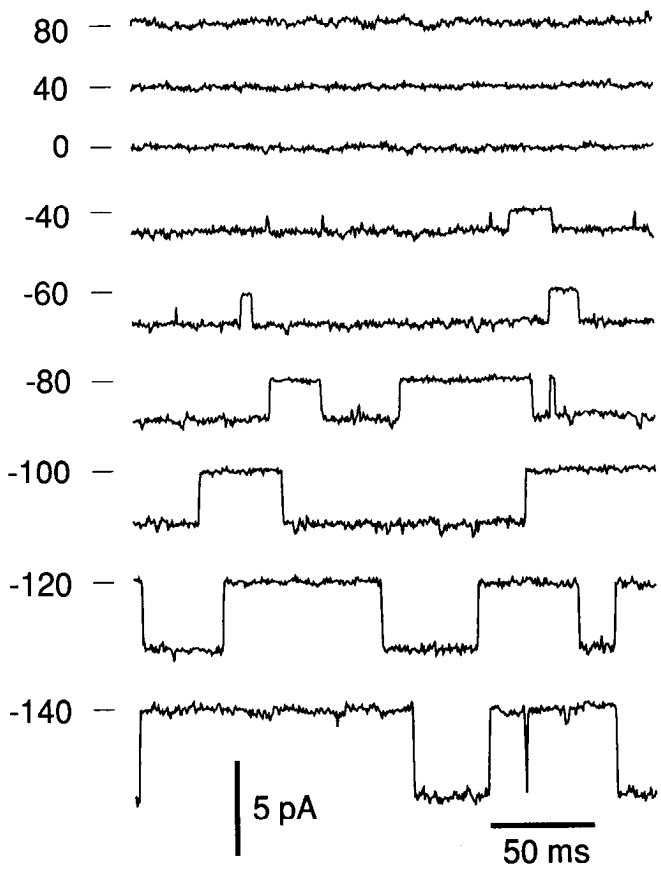

Figure 8. Single-channel voltage-clamp records of an inward-rectifying K^+ channel. Holding potential values (in mV) are given at *left*. *Horizontal line segments* indicate the closed-state current level. The channel remains closed at depolarizing membrane voltages and gates open at hyperpolarizing voltages. Cell-attached membrane patch from near the junction of the endfoot and proximal process.

Single-channel currents

A series of cell-attached, single-channel recordings were made to investigate further the nature of the channels present in Müller cells. These patch-clamp recordings revealed the overwhelming predominance of a single type of channel in all cell regions. This was an inward-rectifying K^+ channel. Voltage-clamp traces from one such recording, made with 98 mM K^+ in the recording pipette, are illustrated in Figure 8. Gated, single-channel currents were present when the cell membrane was hyperpolarized but were absent when the membrane was depolarized. Channel current had a reversal potential near 0 mV, the approximate value of the K^+ equilibrium potential. These properties are typical of inward-rectifying K^+ channels, which conduct inward current for membrane hyperpolarization but do not conduct outward current for membrane depolarization.

(A second type of channel was seen rarely. Only four examples were encountered in the study, during which several hundred inward-rectifying K^+ channels were recorded. The channel had a larger unitary conductance than the inward-rectifying channel and a low open probability and rapid flickering kinetics at hyperpolarized voltages. This channel was not characterized in detail.)

Inward-rectifying K^+ channels were present in all cell regions tested, including the soma, proximal process, and endfoot of Müller cells. Channel density was low in the soma region where channels were absent in many patches. Channel density was high in the endfoot. Most recordings were made near the border of the proximal process and the endfoot, where channel density was best for securing patch recordings having a few channels.

A series of single-channel recordings was made using patch pipette solutions containing 98, 30, or 10 mM K^+. Results from these experiments are summarized in Figure 9, where plots of the mean *I–V* relations of single channels are shown. Mean channel conductances were 27.8 ± 4.9 pS (29), 19.1 ± 1.8 pS (14), and 7.4 ± 0.7 pS (29), respectively, for external solutions containing 98, 30, and 10 mM K^+. The corresponding reversal potentials were −7.2 ± 7.3 mV, −25.7 ± 5.8 mV, and −43.1 ± 9.1 mV.

The *I–V* relations of inward-rectifying K^+ channels behaved similarly to the relations obtained from whole-cell voltage clamp (Fig. 5). As the external $[K^+]$ was lowered, the single-channel conductance was reduced and the reversal potential shifted in a hyperpolarizing direction. The reduction in channel conductance followed the square root relation closely (graph not shown). However, the shift in reversal potential had a slope of 36.2 mV per decade change in $[K^+]_o$, deviating from the Nernstian ideal to a significant degree. The reason for this deviation is not clear.

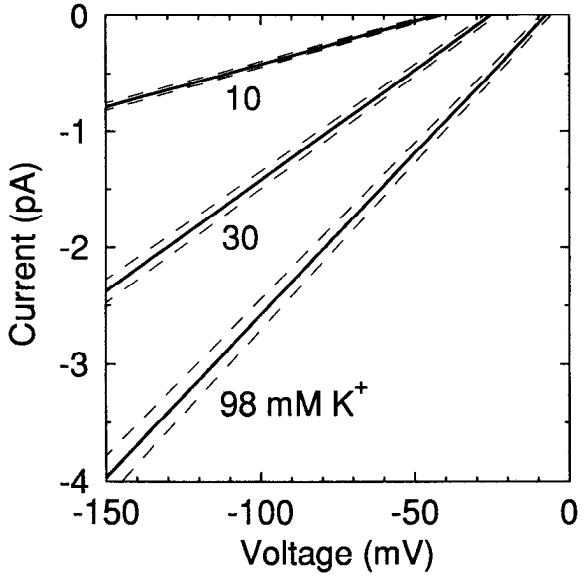

Figure 9. Summary of single-channel *I–V* relations with 98, 30, and 10 mM K^+ in the external (pipette) solution. Mean *I–V* relations ± SEM are shown. *Trace labels* indicate the K^+ concentration (in mM).

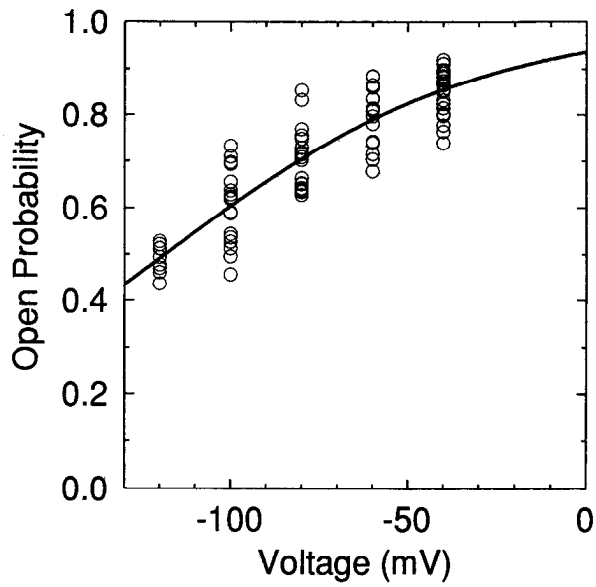

Figure 10. Open probability of inward-rectifying K^+ channels as a function of membrane holding potential. The Boltzmann relation (Eq. 8) is fit to the mean open probability at each potential. Boltzmann parameter values are V_h^p, −118.6 mV; S^p, 44.12 mV.

Single-channel open probability

The records of Figure 8 illustrate that the inward-rectifying K^+ channel is continually closed at voltages more positive than E_K (0 mV in this case). This closure is most likely due to an internal Mg^{2+} block of the channel, as is the case for inward-rectifying K^+ channels in some other systems (Matsuda et al., 1987; Vandenberg, 1987; Matsuda, 1991). The Mg^{2+} block is absent at voltages more negative than E_K. At these hyperpolarized voltages a second type of channel modulation occurs: voltage-dependent gating. As shown in Figure 8, the open probability of the channel varies as a function of membrane potential. Open probability is high at depolarized voltages (Fig. 8, traces −40, −60) and is reduced as the membrane is hyperpolarized.

The gating behavior of the channel was examined by plotting open probability as a function of membrane voltage (Fig. 10). Records were obtained with a pipette solution containing 98 mM K^+. The mean values of open probability at each potential were fit by the two-state Boltzmann equation, which has often been used to model the voltage dependence of channel gating. The equation has the form

$$P_O = \left[1 + \exp\left(\frac{V_h^p - V}{S^p}\right)\right]^{-1}, \qquad (8)$$

where P_o is the channel open probability, V_h^p is the potential at which P_o is 0.5, V is the membrane potential, and S^p is inversely proportional to the rate at which P_o changes with voltage. The best fit to the data was obtained for V_h^p equals −118.6 mV and S^p equals 44.12 mV. [Although P_o was only determined for $[K^+]_o$ = 98 mM, inward-rectifying K^+ channel P_o has been shown to be independent of $[K^+]_o$ in other glial cell preparations (Brew et al., 1986; McLarnon and Kim, 1989a).]

Time dependence of channel open probability

Whole-cell voltage-clamp records (Fig. 2*A,B*) show that the inward currents produced by large hyperpolarizing pulses peak rapidly and then decay to a sustained level. This decay of inward current arises from the time-dependent gating of inward-rectifying K^+ channels, as shown in experiments where channel open probability is monitored as a function of time following a hyperpolarizing voltage step.

A record from one such cell-attached patch-clamp experiment is shown in shown Figure 11*A*. The patch had five active channels that initially were all open when the command potential was shifted from 0 to −100 mV. After a brief period, some of the channels closed. The mean time-dependent response of these five channels is shown in Figure 11*B*, which is an average of 64 sequential voltage-clamp traces. The inward channel current peaked rapidly and then decayed to a sustained level. For comparison, the cell current produced by the same −100 mV voltage step, recorded using the whole-cell voltage-clamp technique, is shown in Figure 11*C*. The decline in inward current seen in the whole-cell record is similar to that measured from the patch recording.

This comparison was quantified by fitting the voltage-clamp records to the sum of two exponentials. The mean value of the first (shorter) time constant proved to be very similar for patch and whole-cell recordings, indicating that the time dependence of channel open probability does indeed account for the time-dependent decline in inward current seen in whole-cell recordings. Mean values of the first time constant were 26.7 ± 11.8 msec (11) for cell-attached patch records and 24.8 ± 6.6 msec (22) for whole-cell recordings. Values of the second time constant were 372 ± 379 msec (11) and 197 ± 148 msec (22), respectively. (The second time constant of the patch records is not reliable due to the noise of the records.)

Quantitative description of cell I–V *relations*

A quantitative description of the *I–V* properties of Müller cells was obtained by fitting the *I–V* relations of cells bathed in physiological levels of K^+ (Fig. 5*B*) to Equations 4–6 and 9. Equation 9, which specifies the membrane conductance of a Müller cell, incorporates two Boltzmann distribution terms. The first term is taken from Equation 7 and represents the rectification of

inward-rectifying K^+ channels (channel block by Mg^{2+}). The second term is taken from Equation 8 and represents the open probability voltage dependence of inward-rectifying K^+ channels. The product of the two terms (rectification open probability) describes the ensemble channel conductance under steady-state conditions. In addition, Equation 9 specifies that the conductance is proportional to the square root of $[K^+]_o$:

$$g = c \cdot \sqrt{[K^+]_o} \times \left[\left(1 + \exp\left(\frac{\Delta V - V_h^R}{S^R}\right)\right) \cdot \left(1 + \exp\left(\frac{V_h^P - V}{S^P}\right)\right)\right]^{-1}. \quad (9)$$

In order to fit a series of I–V relations to Equations 4–6 and 9, N_{SLOPE} of Equation 6 was first adjusted to produce the best fit for the reversal potentials of the four I–V curves. V_h^P and S^P were set to −118.6 mV and 44.12 mV, respectively, the empirically derived values for the Equation 8 parameters. The parameters V_h^R and S^R, as well as the scaling constant c, were then adjusted to produce the best fit to the four I–V curves.

The relation described by Equations 4–6 and 9 provides an excellent fit to the data. This is illustrated in Figure 5*B* by the four sets of symbols, which precisely overlie the voltage-clamp records for most of their length. The closeness of the fit demonstrates that the square root relation linking $[K^+]_o$ to channel conductance holds well.

A total of 13 series of I–V relations with $[K^+]_o$ = 2.5, 4, 7, and 12 mM were fit by Equations 4–6 and 9. The mean values of V_h^R and S^R obtained were −18.5 ± 19.6 mV and 42.4 ± 7.8 mV, respectively.

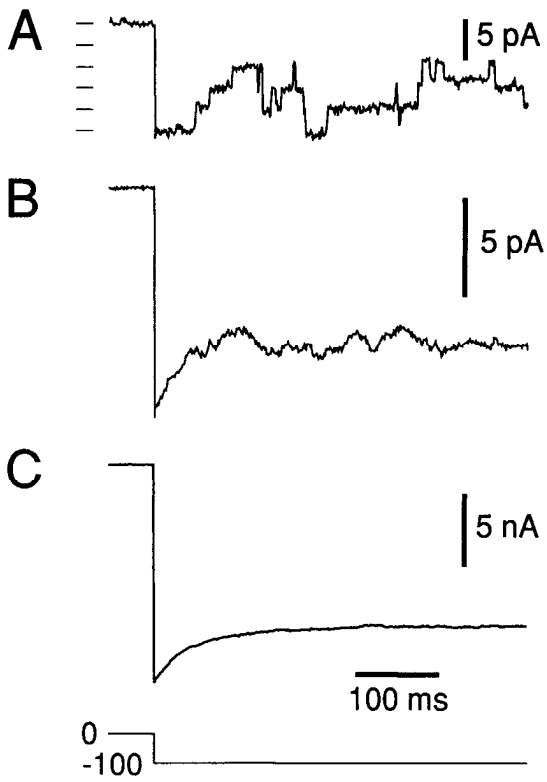

Figure 11. Time dependence of channel open probability. Inward current is evoked by a step change in holding potential from 0 to −100 mV (protocol shown at *bottom*). *A*, Patch-clamp record of a membrane patch containing five inward-rectifying K^+ channels. *Horizontal line segments* indicate single-channel current levels. *B*, Mean current of 64 such records averaged together. Channel open probability is initially high following the voltage step, leading to a large inward current. At later times, open probability decreases, resulting in a reduction in the current. Leakage and capacitive currents were subtracted in *A* and *B*. *C*, Whole-cell voltage-clamp record. Current is evoked by the same −100 mV voltage step. Cell without endfoot. The time course of current decline is similar for single-channel and whole-cell recordings.

Discussion

Inward-rectifying K^+ channels

The results presented here demonstrate clearly that an inward-rectifying K^+ channel is the principal channel type in both endfoot and non-endfoot regions of salamander Müller cells. Three sets of experiments support this conclusion. First, whole-cell I–V relations of both cells without endfeet and cells with endfeet intact displayed prominent inward rectification. Second, the I–V relations of membrane patches from both the soma and endfoot displayed inward rectification. And finally, single-channel patch-clamp recordings showed that an inward-rectifying K^+ channel was the dominant channel type over all Müller cell regions tested.

The properties of the inward-rectifying K^+ channel account well for the observed whole-cell currents of Müller cells. The sustained component of the whole-cell current differed from the peak component at large, hyperpolarizing voltages (Fig. 2*C,D*). This difference is due to the voltage dependence of the channel open probability (Fig. 10), which decreases with increased hyperpolarization. The time course of channel closure following a hyperpolarizing step (Fig. 11*A,B*) matches the time course of the decline in whole-cell current for the same hyperpolarizing voltage step.

The results presented in this work are in good agreement with previous findings. Inward-rectifying K^+ channel currents were first observed in Müller cells in a whole-cell voltage-clamp investigation of amphibian Müller cells without endfeet (Newman, 1985c). A previous single-channel study identified an inward-rectifying K^+ channel as the dominant channel type in both endfoot and soma regions of salamander Müller cells (Brew et al., 1986). These investigators found that the high conductance of the cell endfoot results from a high density of inward-rectifying channels in this cell region. The channel properties described in this earlier single-channel study are very similar to those seen in the present work; unitary conductance was ~31 pS in 89 mM K^+, S^P was ~54 mV, and V_h^P was ~−119 mV. Inward-rectifying channels have also been reported in a patch-clamp study of mammalian Müller cells (Nilius and Reichenbach, 1988). Inward-rectifying K^+ channels are present in mammalian astrocytes (Barres et al., 1990b; Barres, 1991), oligodendrocytes (Barres et al., 1988; Sontheimer and Kettenmann, 1988; McLarnon and Kim, 1989a,b), O-2A glial progenitor cells (Barres et al., 1990a), Schwann cells (Wilson and Chiu, 1990a,b), and glioma cells (Brismar and Collins, 1989), although channel expression in these systems depends on age, culture conditions, and other factors.

The properties of the inward-rectifying K^+ channel described in this work resemble those of other systems. The channel unitary conductance, 27.8 pS in 98 mM K^+, is similar to the conductance in bovine oligodendrocytes, 29 pS in 140 mM K^+ (McLarnon and Kim, 1989a), and in cardiac cells, 27 pS in 145 mM K^+ (Sakmann and Trube, 1984a). The conductance of the Müller cell channel is roughly proportional to the square root

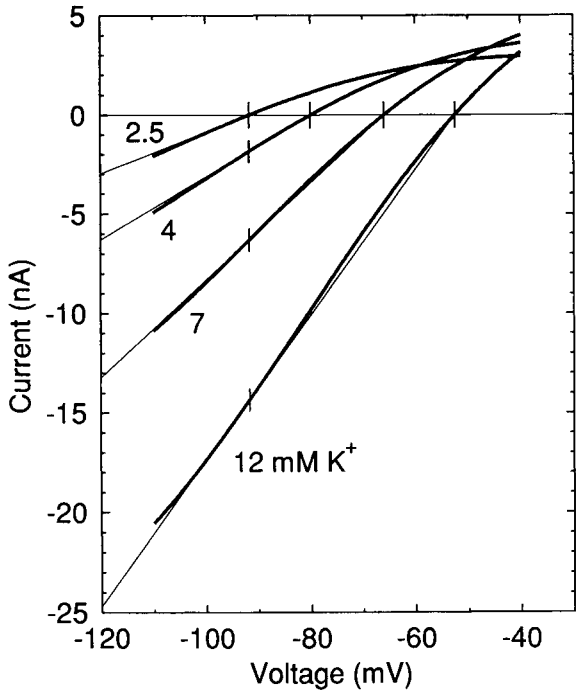

Figure 12. Theoretical *I–V* relations of the "standard" Müller cell bathed in 2.5, 4, 7, and 12 mM K^+ (*thick lines*). The relations are calculated from Equations 4–6 and Equation 10, which specifies the membrane conductance. $[K^+]_i$ = 100 mM and N_{SLOPE} = 25 mV in Equation 6. The cell is assumed to have a conductance of 106 nS for $[K^+]_o$ = 2.5 mM, the mean value measured empirically. The *thin lines* show the chord conductance for each *I–V* plot, calculated at −92 mV, the reversal potential in 2.5 mM K^+. *Vertical line segments* indicate the points on the *I–V* plots through which the chord conductances pass. Labels indicate the external K^+ concentration (in mM).

of $[K^+]_o$, as it is for inward-rectifying channels in other systems (Hagiwara and Takahashi, 1974; Sakmann and Trube, 1984a). The open probability of the Müller cell channel is voltage and time dependent, as is P_o of the cardiac myocyte channel (Sakmann and Trube, 1984b). The Müller cell channel opens rapidly upon hyperpolarization, as does the channel of cardiac myocytes (Sakmann and Trube, 1984a). In contrast, the inward-rectifying channel of the starfish egg activates slowly over several hundred milliseconds (Hagiwara et al., 1976).

Distribution and density of K^+ channels

In the present study, whole-cell inward-rectifying currents were 9.2 times larger in cells with endfeet intact than in cells without endfeet, indicating that 89.2% of the inward-rectifying K^+ channels are localized to the endfoot or to the neighboring proximal process. (This estimate of conductance distribution assumes that cell processes were not lost during the dissociation procedure.) Similarly, multichannel patch-clamp currents recorded from endfoot membrane were substantially larger (an average of 38-fold) than were currents from soma membrane, demonstrating that channel density is far greater on the endfoot. Even in recordings from endfoot membrane, however, there was a wide variation in the number of channels per patch, suggesting that there may be small portions of the endfoot membrane, perhaps only a few micrometers wide, that contain an extremely high density of channels. One endfoot patch had an inward current of −890 pA at −100 mV, equivalent to the current of ~320 active inward-rectifying K^+ channels.

An estimate of the total number of inward-rectifying K^+ channels in a Müller cell can be made by dividing the cell conductance by channel conductance. In bath solution containing 98 mM K^+, the conductance of cells with endfeet averaged 1.49 μS. Thus, there are ~53,600 inward-rectifying K^+ channels per cell. An estimated 89.2% of these channels are localized to the endfoot or proximal process. If we assume a total cell area of 5540 μm^2 and an endfoot area of 442 μm^2 (Newman, 1985b), active channel density on non-endfoot cell regions is 1.14 channels/μm^2 while the density on the endfoot is 109 channels/μm^2. Based on these values, the ratio of channel density on endfoot and non-endfoot membrane is 95:1, even larger than the 38:1 ratio estimated from multichannel patch-clamp records.

Quantitative description of channel properties

A primary goal of this work has been to obtain a quantitative description of the voltage- and $[K^+]_o$-dependent properties of the inward-rectifying K^+ channel of Müller cells. This was accomplished by determining the voltage dependence of channel open probability and by measuring whole-cell *I–V* relations of cells bathed in physiological levels of K^+. These data were then fit by Equations 4–6 and 9.

The empirically derived values of V_h^P, S^P, V_h^R, and S^R can be incorporated into an equation that describes the membrane conductance of a "standard" Müller cell. The equation has the form

$$g = 2.50 \cdot g_{2.5} \sqrt{[K^+]_o} \times \left[\left(1 + \exp\left(\frac{\Delta V + 18.5}{42.4}\right)\right)\cdot\left(1 + \exp\left(\frac{-118.6 - V}{44.1}\right)\right)\right]^{-1}, \quad (10)$$

where $g_{2.5}$ is the cell membrane conductance for $[K^+]_o$ = 2.5 mM. *I–V* relations of the "standard" Müller cell can be plotted from Equations 4–6 and 10, and are shown in Figure 12, for $[K^+]_o$ = 2.5, 4, 7, and 12 mM.

Potassium siphoning

One of the essential functions of glial cells in the CNS is to buffer activity-dependent variations in $[K^+]_o$ (Newman, 1985a; Cserr, 1986). This function is particularly well documented for amphibian Müller cells, which regulate $[K^+]_o$ in the retina by the process of K^+ siphoning (Newman et al., 1984; Karwoski et al., 1989). Light-evoked K^+ increases, which are largest in the inner plexiform layer of the retina (Karwoski and Proenza, 1980; Dick and Miller, 1985; Karwoski et al., 1985), generate an influx of K^+ into Müller cells, leading to cell depolarization. This depolarization induces a K^+ efflux from other cell regions. Because most Müller cell channels lie at the cell endfoot in amphibians, this efflux occurs predominately from the endfoot. Potassium leaving the endfoot diffuses into the adjacent vitreous humor, which functions as a reservoir or sink for the K^+.

The net effect of this process in amphibian species is to transfer K^+ from regions of light-evoked $[K^+]_o$ increase in the retina to the vitreous humor. Ion-selective microelectrode measurements of $[K^+]_o$ in the vitreous and within the retina (Karwoski et al., 1989) have confirmed that this K^+ siphoning mechanism plays a dominant role in the removal of K^+ from the amphibian retina. [The distribution of K^+ channels in mammalian Müller cells is more complex (Newman, 1987) and leads to K^+ siphoning currents directed to other retinal regions (Frishman et al., 1992).]

The effectiveness of the K^+ siphoning process is limited, in

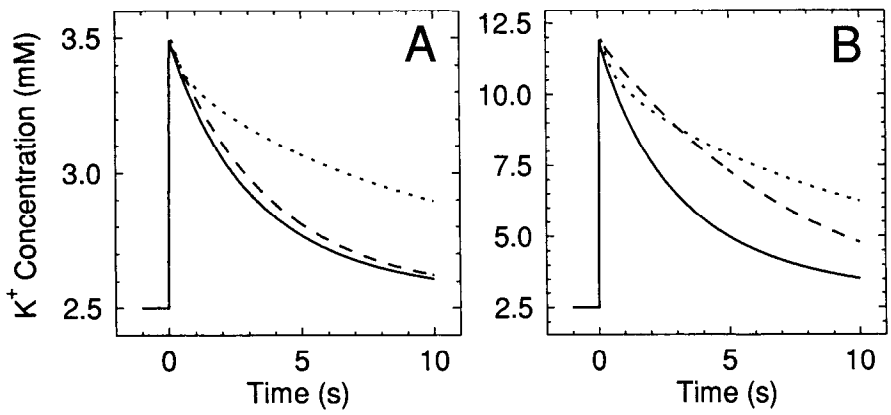

Figure 13. Simulations of K^+ clearance from the retina. At $t = 0$, $[K^+]_o$ is raised from 2.5 mM to 3.5 mM (*A*) or to 12 mM (*B*) within the inner plexiform layer. The plots show the subsequent clearance of K^+ from the inner plexiform layer. Three clearance mechanisms are simulated: K^+ siphoning with inward-rectifying K^+ channels (*continuous lines*), K^+ siphoning with ohmic K^+ channels (*dashed lines*), and K^+ diffusion through extracellular space (*dotted lines*). Clearance occurs most rapidly for K^+ siphoning with inward-rectifying channels.

large part, by the low density of K^+ channels in the non-endfoot regions of Müller cells (Newman et al., 1984; Brew and Attwell, 1985; Eberhardt and Reichenbach, 1987). The sparseness of channels limits the influx of K^+ into Müller cells and restricts the total amount of K^+ that can be transferred by the siphoning process.

However, influx of K^+ into Müller cells is controlled by channel conductance as well as by channel density. As we have seen, the ensemble conductance of inward-rectifying K^+ channels is a function of both voltage and $[K^+]_o$. As described in the following paragraphs, the voltage- and $[K^+]_o$-dependent properties of these channels result in an increase in channel conductance in regions where $[K^+]_o$ is raised.

The increase in inward-rectifying channel conductance is best analyzed by considering the *I–V* plots of the archetypic Müller cell bathed in 2.5, 4, 7, and 12 mM K^+ (Fig. 12, thick lines). The resting membrane potential of the cell in 2.5 mM K^+ is approximately −92 mV. The membrane conductance of the cell in 2.5 mM K^+ is given by the slope conductance (thin line) of the 2.5 mM *I–V* plot at the cell resting potential. The conductance is 106 nS.

Let us now consider the conductance of a small region of non-endfoot membrane that is exposed to 4 mM K^+ (generated by the activity of neighboring neurons). If we assume that the region of increased $[K^+]_o$ is restricted, the cell resting potential will remain at −92 mV. Under these conditions, the conductance of the region of membrane experiencing the 4 mM K^+ is given by the chord conductance of the 4 mM *I–V* plot at −92 mV. This conductance equals 157 nS. Similar calculations can be made for $[K^+]_o$ increases to 7 mM and to 12 mM, and yield chord conductances of 245 nS and 366 nS, respectively. When expressed as a ratio, the membrane conductance in 2.5, 4, 7, and 12 mM K^+ varies as 1:1.49:2.31:3.46.

These conductance increases have an important bearing on the regulation of K^+ by Müller cells. An increase in membrane conductance in regions of raised $[K^+]_o$ will augment the influx of K^+ into Müller cells in these regions. Increased K^+ influx, in turn, will lead to enhanced transfer of K^+ by the siphoning process and to better regulation of $[K^+]_o$. Note that a rise in membrane conductance occurs only in regions where $[K^+]_o$ is raised. Thus, K^+ efflux during the siphoning process will continue to be localized to the cell endfoot.

Potassium clearance in the retina

The precise degree to which increased $[K^+]_o$ augments K^+ siphoning currents is difficult to assess. The increases in cell membrane conductance calculated above assume that the Müller cell membrane potential does not change when $[K^+]_o$ is raised. It is well known, however, that light-evoked $[K^+]_o$ increases in the retina do depolarize Müller cells (by a few millivolts) (Karwoski and Proenza, 1977). Thus, actual increases in membrane conductance will be somewhat less than those calculated above.

In light of this and other complicating factors, I have chosen to evaluate the effect of inward-rectifying channels on K^+ siphoning by using a model of K^+ dynamics in the retina (Odette and Newman, 1988). The model simulates the regulation of K^+ by a siphoning current flow in Müller cells. Müller cell K^+ conductance is specified in the model, either as an ohmic conductance or as an inward-rectifying conductance described by Equation 10. Müller cell depolarization due to $[K^+]_o$ increases is simulated in the model, as is diffusion of K^+ through extracellular space and the release of K^+ from active neurons.

The model was used to simulate the clearance of K^+ from the amphibian retina following a simple step change in $[K^+]_o$. Potassium concentration was initially set to 2.5 mM throughout the retina and in the vitreous humor. At time = 0, $[K^+]_o$ was raised instantaneously within the inner plexiform layer, a region extending from 45 μm to 95 μm beneath the vitreal surface of the retina. Clearance of this $[K^+]_o$ increase from the inner plexiform layer (measured at a depth of 70 μm) was then followed in time. Two simulations were run, with $[K^+]_o$ in the inner plexiform layer raised from 2.5 mM either to 3.5 mM (Fig. 13*A*) or to 12 mM (Fig. 13*B*).

Three distinct clearance mechanisms were analyzed in the simulations: (1) clearance via K^+ siphoning with inward-rectifying Müller cell channels (Fig. 13, continuous lines), (2) clearance via K^+ siphoning with ohmic Müller cell channels (Fig. 13, dashed lines), and (3) clearance via K^+ diffusion through extracellular space (Fig. 13, dotted lines). The effect of each of these buffering mechanisms on clearance of the $[K^+]_o$ increase was analyzed independently of the other two.

The simulations demonstrate that K^+ clearance occurs most rapidly for K^+ siphoning with inward-rectifying channels, somewhat slower for K^+ siphoning with ohmic channels, and slowest of all for simple diffusion. The enhancement of the K^+ siphoning process by inward-rectifying channels is far more pronounced for a $[K^+]_o$ increase to 12 mM (Fig. 13*B*) than for an increase to 3.5 mM (Fig. 13*A*). This is expected since the increase in inward-rectifying channel conductance is greater for larger $[K^+]_o$ increases.

The simulations can be analyzed by determining the time taken to reduce the $[K^+]_o$ increase to one-half its initial value.

For a K^+ increase to 3.5 mM (Fig. 13*A*) the one-half clearance time is 2.42 sec for siphoning with inward-rectifying channels, 2.87 sec for siphoning with ohmic channels, and 6.66 sec for diffusion. Corresponding one-half clearance times for an increase to 12 mM (Fig. 13*B*) are 2.32 sec, 5.08 sec, and 6.66 sec. Thus, inward-rectifying channels augment K^+ siphoning moderately for a 1 mM K^+ increase (a 16% decrease in one-half clearance time), but enhance K^+ siphoning substantially for a 9.5 mM K^+ increase (a 54% decrease in the one-half clearance time).

The enhancement of K^+ siphoning by inward-rectifying K^+ channels can also be assessed by examining the initial clearance rates (the slope of the plots at time = 0). For the K^+ increase to 3.5 mM, the initial clearance rates are 0.28 and 0.23 mM/sec for inward-rectifying and ohmic K^+ channels, respectively. Corresponding clearance rates for 12 mM K^+ are 2.82 and 1.19 mM/sec. Thus, the clearance rate is enhanced 23% for a 1 mM K^+ increase and 137% for a 9.5 mM increase.

The simulations demonstrate that inward-rectifying channels enhance the K^+ siphoning process in Müller cells in response to activity-dependent increases in $[K^+]_o$. This results in better regulation of $[K^+]_o$ in the retina than would be possible if the K^+ channels of Müller cells were ohmic.

Light-evoked $[K^+]_o$ increases in the retina rarely exceed 1 mM (Karwoski and Proenza, 1980; Dick and Miller, 1985). Thus, K^+ siphoning is, most likely, enhanced only moderately by Müller cell inward-rectifying channels. However, even a 20% or 30% increase in clearance rate may play an important role in maintaining proper retinal function. [Retinal $[K^+]_o$ can increase to 30–50 mM during experimentally induced spreading depression episodes (Mori et al., 1976; do Carmo and Martins-Ferreira, 1984). Unlike the cerebral cortex, however, it is not clear whether spreading depression occurs naturally in the *in vivo* retina.]

The situation is different in the brain (Somjen, 1979; Sykova, 1983). As in the retina, sensory stimulation results in modest $[K^+]_o$ increases, rarely exceeding 1 mM (Kelly and Van Essen, 1974; Singer and Lux, 1975). However, $[K^+]_o$ can rise dramatically under pathological conditions. Potassium concentration increases to 8–12 mM during epileptic discharges (Lux, 1974; Lothman et al., 1975) and rises to 30–80 mM during episodes of spreading depression (Lothman et al., 1975; Nicholson et al., 1978). Like Müller cells, astrocytes (and perhaps oligodendrocytes) regulate $[K^+]_o$ variations by a spatial buffering and/or K^+ siphoning process (Orkand et al., 1966; Gardner-Medwin, 1983, 1986; Newman, 1986; Dietzel et al., 1989). Potassium currents in these cells are likely carried by inward-rectifying K^+ channels (Barres, 1991). The voltage- and K^+-dependent properties of these channels could substantially enhance the K^+ buffering function of glial cells in the brain.

References

Barres BA (1991) New roles for glia. J Neurosci 11:3685–3694.

Barres BA, Chun LLY, Corey DP (1988) Ionic channel expression by white matter glia: I. Type 2 astrocytes and oligodendrocytes. Glia 1:10–30.

Barres BA, Koroshetz WJ, Swartz KJ, Chun LLY, Corey DP (1990a) Ion channel expression by white matter glia: the O-2A glial progenitor cell. Neuron 4:507–524.

Barres BA, Koroshetz WJ, Chun LLY, Corey DP (1990b) Ion channel expression by white matter glia: the type-1 astrocyte. Neuron 5:527–544.

Brew H, Attwell D (1985) Is the potassium channel distribution in glial cells optimal for spatial buffering of potassium. Biophys J 48: 843–847.

Brew H, Gray PTA, Mobbs P, Attwell D (1986) Endfeet of retinal glial cells have higher densities of ion channels that mediate K^+ buffering. Nature 324:466–468.

Brismar T, Collins VP (1989) Inward-rectifying potassium channels in human malignant glioma cells. Brain Res 480:249–258.

Cserr HF (1986) The neuronal microenvironment. Ann NY Acad Sci 481:1–393.

Dick E, Miller RF (1985) Extracellular K^+ activity changes related to electroretinogram components. I. Amphibian (I-type) retinas. J Gen Physiol 85:885–909.

Dietzel I, Heinemann U, Lux HD (1989) Relations between slow extracellular potential changes, glial potassium buffering, and electrolyte and cellular volume changes during neuronal hyperactivity in cat brain. Glia 2:25–44.

do Carmo RJ, Martins-Ferreira H (1984) Spreading depression of Leao probed with ion-selective microelectrodes in isolated chick retina. An Acad Brasil Cienc 56:401–421.

Eberhardt W, Reichenbach A (1987) Spatial buffering of potassium by retinal Muller (glial) cells of various morphology calculated by a model. Neuroscience 22:687–696.

Frishman LJ, Yamamoto F, Bogucka J, Steinberg RH (1992) Light-evoked changes in $[K^+]_o$ in proximal portion of light-adapted cat retina. J Neurophysiol 67:1201–1212.

Gardner-Medwin AR (1983) Analysis of potassium dynamics in mammalian brain tissue. J Physiol (Lond) 335:393–426.

Gardner-Medwin AR (1986) A new framework for assessment of potassium-buffering mechanisms. Ann NY Acad Sci 481:287–302.

Hagiwara S (1983) Membrane potential-dependent ion channels in cell membrane. New York: Raven.

Hagiwara S, Takahashi K (1974) The anomalous rectification and cation selectivity of the membrane of a starfish egg cell. J Membr Biol 18:61–80.

Hagiwara S, Miyazaki S, Rosenthal NP (1976) Potassium current and the effect of cesium on this current during anomalous rectification of the egg cell membrane of a starfish. J Gen Physiol 67:621–638.

Hamill OP, Marty A, Neher E, Sakmann B, Sigworth FJ (1981) Improved patch-clamp techniques for high-resolution current recording from cells and cell-free membrane patches. Pfluegers Arch 391:85–100.

Hille B (1992) Ionic channels of excitable membranes. Sunderland, MA: Sinauer.

Karwoski CJ, Proenza LM (1977) Relationship between Muller cell responses, a local transretinal potential, and potassium flux. J Neurophysiol 40:244–259.

Karwoski CJ, Proenza LM (1980) Neurons, potassium, and glia in proximal retina of *Necturus*. J Gen Physiol 75:141–162.

Karwoski CJ, Newman EA, Shimazaki H, Proenza LM (1985) Light-evoked increases in extracellular K^+ in the plexiform layers of amphibian retinas. J Gen Physiol 86:189–213.

Karwoski CJ, Lu H-K, Newman EA (1989) Spatial buffering of light-evoked potassium increases by retinal Müller (glial) cells. Science 244: 578–580.

Kelly JP, Van Essen DC (1974) Cell structure and function in the visual cortex of the cat. J Physiol (Lond) 238:515–547.

Kuffler SW, Nicholls JG, Orkand RK (1966) Physiological properties of glial cells in the central nervous system of amphibia. J Neurophysiol 29:768–787.

Lothman E, LaManna J, Cordingley G, Rosenthal M, Somjen G (1975) Responses of electrical potential, potassium levels, and oxidative metabolic activity of the cerebral neocortex of cats. Brain Res 88:15–36.

Lux HD (1974) The kinetics of extracellular potassium: relation to epileptogenesis. Epilepsia 15:375–393.

Maranto AR, Newman EA (1988) Endfeet of retinal glial (Müller) cells have a non-rectifying K^+ conductance. Soc Neurosci Abstr 14:585.

Matsuda H (1991) Magnesium gating of the inwardly rectifying K^+ channel. Annu Rev Physiol 53:289–298.

Matsuda H, Saigusa A, Irisawa H (1987) Ohmic conductance through the inwardly rectifying K^+ channel and blocking by internal Mg^{2+}. Nature 325:156–159.

McLarnon JG, Kim SU (1989a) Single channel potassium currents in cultured adult bovine oligodendrocytes. Glia 2:298–307.

McLarnon JG, Kim SU (1989b) Existence of inward potassium currents in adult human oligodendrocytes. Neurosci Lett 101:107–112.

Mori S, Miller WH, Tomita T (1976) Microelectrode study of spreading depression (SD) in frog retina—Muller cell activity and $[K^+]$ during SD. Jpn J Physiol 26:219–233.

Newman EA (1984) Regional specialization of retinal glial cell membrane. Nature 309:155–157.
Newman EA (1985a) Regulation of potassium levels by glial cells in the retina. Trends Neurosci 8:156–159.
Newman EA (1985b) Membrane physiology of retinal glial (Müller) cells. J Neurosci 5:2225–2239.
Newman EA (1985c) Voltage-dependent calcium and potassium channels in retinal glial cells. Nature 317:809–811.
Newman EA (1986) High potassium conductance in astrocyte endfeet. Science 233:453–454.
Newman EA (1987) Distribution of potassium conductance in mammalian Müller (glial) cells: a comparative study. J Neurosci 7:2423–2432.
Newman EA (1989a) Potassium conductance block by barium in amphibian Müller cells. Brain Res 498:308–314.
Newman EA (1989b) Inward-rectifying potassium channels in retinal glial (Müller) cells. Soc Neurosci Abstr 15:353.
Newman EA, Frambach DA, Odette LL (1984) Control of extracellular potassium levels by retinal glial cell K^+ siphoning. Science 225:1174–1175.
Nicholson C, ten Bruggencate G, Stockle H, Steinberg R (1978) Calcium and potassium changes in extracellular microenvironment of cat cerebellar cortex. J Neurophysiol 41:1026–1039.
Nilius B, Reichenbach A (1988) Efficient K^+ buffering by mammalian retinal glial cells is due to cooperation of specialized ion channels. Pfluegers Arch 411:654–660.
Odette LL, Newman EA (1988) Model of potassium dynamics in the central nervous system. Glia 1:198–210.
Oliva C, Cohen IS, Pennefather P (1990) The mechanism of rectification of i_{K1} in canine Purkinje myocytes. J Gen Physiol 96:299–318.
Orkand RK, Nicholls JG, Kuffler SW (1966) Effect of nerve impulses on the membrane potential of glial cells in the central nervous system of amphibia. J Neurophysiol 29:788–806.
Rudy B (1988) Diversity and ubiquity of K channels. Neuroscience 25:729–749.
Sakmann B, Trube G (1984a) Conductance properties of single inwardly rectifying potassium channels in ventricular cells from guinea-pig heart. J Physiol (Lond) 347:641–657.
Sakmann B, Trube G (1984b) Voltage-dependent inactivation of inward-rectifying single-channel currents in the guinea-pig heart cell membrane. J Physiol (Lond) 347:659–683.
Singer W, Lux HD (1975) Extracellular potassium gradients and visual receptive fields in the cat striate cortex. Brain Res 96:378–383.
Somjen GG (1979) Extracellular potassium in the mammalian central nervous system. Annu Rev Physiol 41:159–177.
Sontheimer H, Kettenmann H (1988) Heterogeneity of potassium currents in cultured oligodendrocytes. Glia 1:415–420.
Sykova E (1983) Extracellular K^+ accumulation in the central nervous system. Prog Biophys Mol Biol 42:135–189.
Vandenberg CA (1987) Inward rectification of a potassium channel in cardiac ventricular cells depends on internal magnesium ions. Proc Natl Acad Sci USA 84:2560–2564.
Wilson GF, Chiu SY (1990a) Potassium channel regulation in Schwann cells during early developmental myelinogenesis. J Neurosci 10:1615–1625.
Wilson GF, Chiu SY (1990b) Ion channels in axon and Schwann cell membranes at paranodes of mammalian myelinated fibers studied with patch clamp. J Neurosci 10:3263–3274.